

## All-natural bio-plastics using starch-betaglucan composites

Domenico Sagnelli <sup>a,\*</sup>, Jacob J.K. Kirkensgaard <sup>b</sup>, Concetta Valeria L. Giosafatto <sup>c</sup>, Natalia Ogrodowicz <sup>d</sup>, Krzysztof Kruczak <sup>e</sup>, Mette S. Mikkelsen <sup>f</sup>, Jean-Eudes Maigret <sup>g</sup>, Denis Lourdin <sup>g</sup>, Kell Mortensen <sup>b</sup>, Andreas Blennow <sup>a,\*</sup>

<sup>a</sup> Department of Plant and Environmental Sciences, University of Copenhagen, Denmark

<sup>b</sup> Niels Bohr Institute, University of Copenhagen, Copenhagen, Denmark

<sup>c</sup> Department of Chemical Science, University of Naples Federico II, Napoli, Italy

<sup>d</sup> Jerzy Haber Institute of Catalysis and Surface Chemistry Polish Academy of Sciences, Kraków, Poland

<sup>e</sup> Faculty of Chemistry, Jagiellonian University, Kraków, Poland

<sup>f</sup> Department of Food Science, University of Copenhagen, Frederiksberg C, Denmark

<sup>g</sup> Institut National De La Recherche Agronomique, Nantes, France



### ARTICLE INFO

#### Article history:

Received 17 February 2017

Received in revised form 15 May 2017

Accepted 15 May 2017

Available online 20 May 2017

#### Keywords:

Starch

Beta-glucan

Bio-plastics

Composites

Barrier properties

### ABSTRACT

Grain polysaccharides represent potential valuable raw materials for next-generation advanced and environmentally friendly plastics. Thermoplastic starch (TPS) is processed using conventional plastic technology, such as casting, extrusion, and molding. However, to adapt the starch to specific functionalities chemical modifications or blending with synthetic polymers, such as polycaprolactone are required (e.g. Mater-Bi). As an alternative, all-natural and compostable bio-plastics can be produced by blending starch with other polysaccharides. In this study, we used a maize starch (ST) and an oat  $\beta$ -glucan (BG) composite system to produce bio-plastic prototype films. To optimize performing conditions, we investigated the full range of ST:BG ratios for the casting (100:0, 75:25, 50:50, 25:75 and 0:100 BG). The plasticizer used was glycerol. Electron Paramagnetic Resonance (EPR), using TEMPO (2,2,6,6-tetramethylpiperidine-1-oxyl) as a spin probe, showed that the composite films with high BG content had a flexible chemical environment. They showed decreased brittleness and improved cohesiveness with high stress and strain values at the break. Wide-angle X-ray diffraction displayed a decrease in crystallinity at high BG content. Our data show that the blending of starch with other natural polysaccharides is a noteworthy path to improve the functionality of all-natural polysaccharide bio-plastics systems.

© 2017 Elsevier Ltd. All rights reserved.

### 1. Introduction

Thermoplastic starch (TPS) is a bio-based material with the potential to become a future biodegradable and every-day-use bio-plastic. Several recent studies have pinpointed TPS materials and composites as possible targets for new short- and medium-life bio-plastics. The reasons are its simple chemical structure, the desirable physiochemical properties, the abundance in nature and the well-established production technologies (Jantanasakulwong et al., 2016; Montero, Rico, Rodríguez-Llamazares, Barral & Bouza, 2016; Sagnelli et al., 2016). Starch (ST) comprises two major polymers, amylose and amylopectin, which differ in branching and molecular size. Amylose is a chiefly linear polymer composed of  $\alpha(1\text{-}4)$ -linked glucose units and a molecular weight

(Mw) of about  $10^5\text{--}10^6\text{ g mol}^{-1}$ . Amylopectin is a larger molecule ( $Mw=10^7\text{--}10^9\text{ g mol}^{-1}$ ) and is a branched polymer with a  $\alpha(1\text{-}4)$ -linked glucose backbone and typically 5%  $\alpha(1\text{-}6)$ -linked branches (Blennow et al., 2013). The higher structural level does not show this molecular simplicity. In fact, complex structures are found because of the different assembly of the linear segments of the starch. Thus, starch is organized as a semi-crystalline polymer organized in granules whose dimensions and microstructure are variable. In the starch granules, the linear segments of the amylopectin chains are organized in discrete crystalline polymorphs. These crystals are dependent on both the botanical origin and processing. As determined by wide angle X-ray diffraction (WAXS) there are three main crystalline structures termed A-type, B-type and Vh-type crystalline polymorphs (Pérez, Baldwin, & Gallant, 2009). These polymorphs are interchanged during bio-plastics fabrication (Sagnelli et al., 2016).

The semi-crystalline nature of starch can persist after materials fabrication and so influences the final properties of the material produced. In fact, after melting of the polymer, a recrystallization

\* Corresponding authors.

E-mail addresses: [dsagnelli@plen.ku.dk](mailto:dsagnelli@plen.ku.dk), [domenico.sagnelli@gmail.com](mailto:domenico.sagnelli@gmail.com) (D. Sagnelli), [abl@plen.ku.dk](mailto:abl@plen.ku.dk) (A. Blennow).

phase takes place during the cooling process. This phase leads the material through an aging progression including various degrees of retrogradation (recrystallization) of the starch. Starch is a polar polymer producing a poorly cohesive and highly brittle material (Follain, Joly, Dole, & Bliard, 2005). To overcome these problems, a plasticizer, for example glycerol, is added to increase flexibility and reduce brittleness (Giosafatto et al., 2014a, 2014b). The plasticization enables the material to tolerate increased strain, but it also decreases the strength of the material (Lourdin, Della Valle, & Colonna, 1995; Myllarinen, Partanena, Seppala, & Forssell, 2002). Different approaches are used to improve TPS functionality. Only a few of them are focused on all-natural components. This is demanding and an interesting new concept is to produce the so-called plant-crafted starches modified directly in the seed by using transgenic technology to increase flexibility (Hebelstrup, Sagnelli, & Blennow, 2015; Sagnelli et al., 2016).

An alternative is the use of composites consisting of blends of starch with other natural or synthetic polymers. Elasticity and cohesiveness are enhanced in starch by chemical modification or by blending with synthetic polymers, such as polycaprolactone (Bastioli, Bellotti, Del Giudice, & Grilli, 1993). However, to create an eco-friendly material, the starch can be blended with other natural polymers such as proteins or other polysaccharides. This approach could enhance its original properties or add new ones, generating all-natural blend systems. An example is the  $\beta(1\text{-}3)\beta(1\text{-}4)$  mixed-linkage beta-glucan (BG) occurring in grains of oat and barley. This polysaccharide is a multifunctional dietary fiber with food health benefits (Gemen, de Vries, & Slavin, 2011; Lazaridou & Biliaderis, 2007; Lazaridou, Biliaderis, Micha-Screttas & Steele, 2004; Mikkelsen, Jespersen, Larsen, Blennow, & Engelsen, 2013). BG is one of the major non-cellulosic polysaccharides in the grasses (Burton & Fincher, 2012).  $\beta(1\text{-}3)\beta(1\text{-}4)$  mixed-linkage beta-glucan structure is composed of cellobiosyl ( $\beta(1\text{-}4)$ , DP3) and cellobetaosyl ( $\beta(1\text{-}4)$ , DP4) residues linked by single  $\beta(1\text{-}3)$  linkages (Burton & Fincher, 2012). The relative distribution and amounts of the triosyl, tetraosyl and longer blocks along the BG chain are essential for the physical aggregation and solubility of the BG. As an effect, the repetitive structures in BG causes more aggregation and lower solubility (Burton & Fincher, 2012; Mikkelsen et al., 2013).  $\beta(1\text{-}4)$  linked block segments provide structural resemblance to cellulose and could make this polysaccharide a protagonist in material science.

In this study, we established maize ST and oat BG as an all-natural bio-composite system using different ST:BG proportions. Prototype films manufactured by casting and tested for crystallinity, dynamic mechanical analysis (DMA), electron paramagnetic resonance (EPR) and mechanical properties had different functionality characterized mainly by decreased brittleness and improved cohesiveness and decreased crystallinity. The study shows the potential of using natural plant polysaccharides to modulate the properties of the starch-based bio-plastics.

## 2. Materials and method

### 2.1. Materials

The BG was derived from an oat  $\beta$ -glucan concentrate (PromOat<sup>TM</sup>, Biovelop, Kimstad, Sweden). Cerestar-AKV I/S (Vodskov, Denmark) kindly offered the maize starch, the starch contained 10–13% water 0.3% proteins, 0.1% fat and virtually no fibers (product specifications). All chemicals were from Sigma-Aldrich.

### 2.2. Methods

#### 2.2.1. Beta-glucan extraction

BG extracts from a large-scale extraction were used in the experiments (Mikkelsen et al., 2013). Briefly, the purification was

performed as follows: extraction with water (5%, w/v) at 95 °C; hydrolysis of ST and proteins using  $\alpha$ -amylase (Thermamyl SC) and protease (Alcalase AF 2.4L) from Novozymes (Bagsværd, Denmark); fractionation using decanting and centrifugation; precipitation of BG from the solution with ethanol and freeze drying of the pellet. The purified oat BG powder contained 73% soluble  $\beta$ -glucan, 5% insoluble fibres, 6% ST and 1% protein. The BG molecular weight was 270 kDa and the molar ratio of tri- and tetrasaccharide blocks in the polysaccharide was 2.2 (Mikkelsen et al., 2013).

#### 2.2.2. Casting of composites films

The different formulations of ST, BG and glycerol were prepared and homogenized using pestle and mortar. The native water content of the ST and BG was measured by a thermogravimetric balance (TG 209 F1 Libra, Netzsch) and taken into account in the preparation of the mixtures. The formulations consisted of the two polysaccharides mixed at different ratios keeping the final polysaccharide mass constant. The ratio of ST:BG in study were: 100:0, 75:25, 50:50, 25:75 and 0:100. The films are denoted using the ST:BG ratio and the content of glycerol. The first number referred to ST, the second to BG and the third number to the glycerol content, e.g. 25:75-0 refers to the film having a ratio between ST:BG of 25:75 and 0% of glycerol. The pure ST film and pure BG film were indicated respectively ST100 and BG100. Glycerol was omitted or added at 23% and 30% (dry weight, d.w.), without affecting the ST:BG ratio. Before the heating treatment, the mixtures were stored at 4 °C for 24 h to achieve equilibrium between the phases. Afterward, 2% w/w solutions were prepared with milliQ water. These solutions were pre-mixed for 1 h at 25 °C in a thermostated oil bath and then mixed for 1 h at 95 °C to gelatinize ST and solubilize the BG. The solutions were cooled while stirring on ice to approximately 70 °C and immediately casted in teflon-coated petri dishes at a surface density of 20 mg/cm<sup>2</sup>. The films were dried at 60 °C in an oven with ventilation. The films were equilibrated for one week in a desiccator containing a saturated solution of sodium bromide (RH 57%±1) prior the analysis.

#### 2.2.3. X-ray scattering

Film prototypes equilibrated at RH 57%±1 (sodium bromide saturated solution) and 75%±1 (potassium hydroxide saturated solution) were sealed between thin mica films to minimize evaporation during the measurement, which was performed in vacuum. X-ray measurements were conducted at the Niels Bohr Institute using a Small Angle X-ray Scattering (SAXS) instrument at the University of Copenhagen. This instrument is equipped with a 100XL+ micro-focus sealed X-ray tube from Rigaku producing a photon beam with a wavelength of 1.54 Å. The scattering patterns were recorded with a 2D 300 K Pilatus detector from Dectris. The two-dimensional scattering data were azimuthally averaged, normalized by the incident radiation intensity, the sample exposure time and the transmission and corrected for background and detector inhomogeneities using standard reduction software (SAXSGUI). The radially averaged intensity  $I = 4\pi \int_0^\infty I(q) q^2 dq$  is given as a function of the scattering vector  $q = 4\pi \sin \theta / \lambda$ , where  $\lambda$  is the wavelength and  $2\theta$  is the scattering angle. The samples were measured in the WAXS setting (Wide-Angle X-ray Scattering) covering a  $q$ -range from about 0.06–2.2 Å<sup>-1</sup> corresponding to an upper  $2\theta$  value of 31.3° or 2.86 Å. The exposure time was 900 s.

#### 2.2.4. Electron paramagnetic resonance

The samples for the electron paramagnetic resonance (EPR) measurements were soaked in a 5 cm<sup>3</sup> of TEMPO (spin probe) solution (0.0093 mol/L) for 6 h, rinsed three times with distilled water and dried overnight in an oven at 50–55 °C. The measurements were performed at 300 K using the Bruker Elexsys E-500 spectrometer operating at X-band (9.5 GHz) and 100 kHz magnetic field

modulation, equipped with the ER 4111 VT variable temperature unit and super high sensitivity cavity ER 4122 SHQE. The spectra were recorded at 2 mW microwave power and 1 G amplitude modulation. The ESR spectra were simulated using the EasySpin package version 5.1.9 available at [www.easyspin.org](http://www.easyspin.org). The software is based on Matlab (Matlab, version R2016b) and includes several functions performing common simulation tasks including “chili” and “garlic” for slow motion and fast-motion EPR spectra, respectively. An interactive least square fitting method (Nelder/Mead Simplex) was used to obtain the best fits.

### 2.2.5. Mechanical properties

Tensile tests of the prototypes were carried out on casted samples cut in a rectangular (base = 3, height = 10 mm, thickness = varied as a function of the mixture). The specimens were tested using the DMA Q800 (TA Instruments, New Castle, DE, USA) in tension mode adding a ramp force of 5 N/min to 18 N. The elongation and tensile stress at break were measured at 20 °C. Each analysis was performed in triplicate.

### 2.2.6. Dynamic mechanical analysis

Dynamic mechanical analysis (DMA) with temperature gradient was performed using the DMA Q800 (TA Instruments, New Castle, DE, USA) working in tension mode with an amplitude of 0.1% and a frequency of 1 Hz. A standard heating rate of 3 °C min<sup>-1</sup> and a ramp from -50 to 120 °C was used. The experiments were performed on prototypes with a length of 10 mm (Lourdin, Bizot & Colonna, 1997). The glass transition temperature was estimated by comparing the derivative function of the storage modulus and the tan delta ( $\tan\delta$ ) peak.

The analysis in humidity gradient was conducted with a DMA 50N 01dB-Metrawib accessorized with a moisture controller: dry air and wet air (100% RH) were blended in the testing chamber and the RH set by adjusting the two flows.

A standard rectangular shape was cut out from the film using a punch (4.2 mm width and ~15 mm length). The thickness value was derived from the average of three measurements performed using a micrometer screw gauge. The samples were mounted between the two clamps whose distance was measured with a caliper ( $10 \pm 0.05$  mm). The temperature was set to 20 °C; the strain rate was 0.01% with a 1 Hz frequency. The static force applied was equal to 0.5 N. The relative humidity (RH) in the testing chamber was manually increased by steps from around 5% RH to more than 80% RH. The equilibrium was achieved before each increase of RH. The storage modulus (E'), loss modulus (E'') and loss factor ( $\tan\delta$ ) were then measured at each RH level.

### 2.2.7. Differential scanning calorimetry (DSC)

The melting temperature of the native polymers was determined by differential scanning calorimetry (DSC) using a DSC 214 polyma (Netzsch) instrument. Experiments were carried out on aliquots of  $20 \pm 1$  mg of the polymer and placed in stainless steel airtight cells. A single scan was run at 3 °C min<sup>-1</sup> from 0 to 150 °C. The melting temperature was defined from the endotherm peak value (Garcia et al., 1996).

### 2.2.8. Permeability to gasses

$\text{CO}_2$ ,  $\text{O}_2$ , and  $\text{H}_2\text{O}$  permeability was determined using the ASTM Standard Method D 3985 (2010) and F1249 with MultiPerm apparatus (Extra-solution s.r.l., Pisa, Italy) and as described in Mariniello, Giosafatto, Di Pierro, Sorrentino, and Porta (2010). The samples, duplicates of each film, were conditioned for 2 days at 50% RH before measurement. Aluminum masks were used to reduce film test area to 5 cm<sup>2</sup>. The testing was performed at 25 °C under 50% RH.

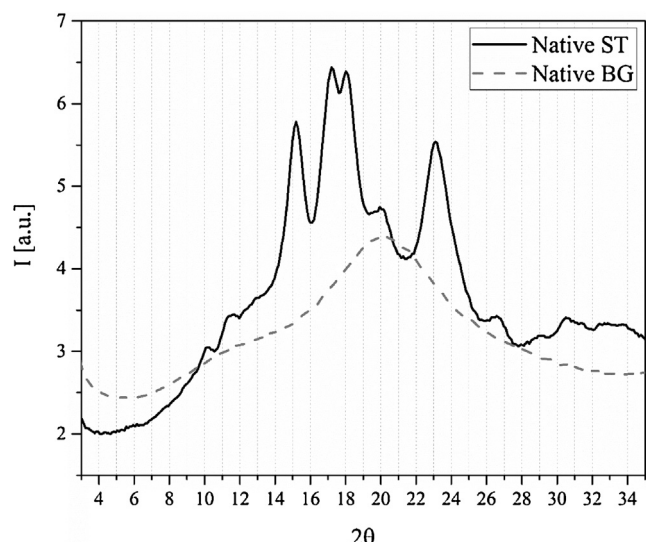


Fig. 1. Diffractograms of raw polysaccharides showing the native crystallinity of ST and BG.

### 2.2.9. Confocal microscopy

Confocal Laser Scanning Microscopy (CLSM) was performed using a Leica system (Leica SP5-X, Leica Microsystems) equipped with x20 water immersion objectives. Films were treated with calcofluor and potassium iodide (Sigma-Aldrich, diluted 10 times) overnight. Calcofluor and iodine fluorescence were analyzed by using laser lines of 365–395 nm or 488 nm for excitation and emitted fluorescence was recorded between 420 nm and 515–650 nm respectively (Ovecka et al., 2012). Images were analyzed with LAS X 3.0.

## 3. Results and discussion

### 3.1. Raw polysaccharides characterization

The raw ST and BG polysaccharides were characterized for their thermal behavior in excess of water using DSC. The ST sample showed a gelatinization peak around 70 °C, typical of native granular starches in excess of water. BG showed no detectable thermal transition. The polysaccharides were then characterized for their crystalline structure with WAXS. Analysis of native ST showed the typical scattering profile related to maize ST crystal polymorph (A-type) (Fig. 1). Measuring the BG, two wide reflections at approximately  $2\theta = 11.3$  and  $19.8^\circ$  (Fig. 1) appeared. These peaks are associated with the 110, 11̄0 and 200 reflections planes from cellulosic microfibrils (cellulose II) crystallites (Hindeleh, 1980; Newman, Hill, & Harris, 2013; Zuluaga Gallego et al., 2014). This corresponds to lattice spacing of 0.45 nm for the 200 reflection and 0.74 nm for the 110 and 11̄0 reflection. These values are higher than the one previously obtained for the cellulose (Newman, Hill & Harris, 2013). This difference may reflect the distances between the  $\beta(1-3)$  linkages interrupting the  $\beta(1-4)$  backbone stretches in BG.

### 3.2. Crystallinity structures and paramagnetic resonance of composites films

Polysaccharide films were fabricated by casting with and without glycerol. The films were characterized for the crystalline structure using WAXS. The possible presence of phases related to different chemical mobility in the films, was monitored using electron paramagnetic resonance (EPR) using TEMPO as a spin probe. The crystallinity measurements of the BG film without glycerol showed the same two peaks as found in the native BG, demon-

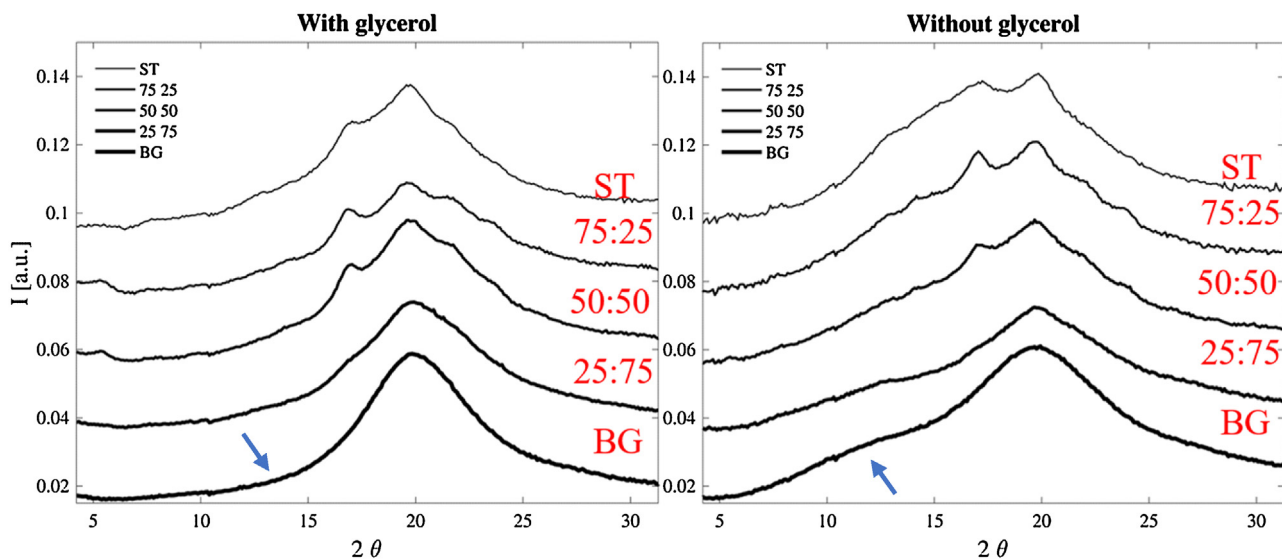


**Fig. 2.** Diffractograms of casted bio-composites film showing the amorphisizing effect of BG on ST films and structural effect of glycerol on the films.

**Table 1**

Extreme separation, line widths and rotational correlation time of nitroxide spin probe obtained from EPR Spectra.

Name of sample	Extreme Separation [G]		F-SC peak to peak width ΔHpp [G]	Rotational correlation time $\tau_c$ [ns]		Relative intensity %F-SC
	S-SC	F-SC		S-SC	F-SC	
ST100-0	67.5	–	4.2	7.3	0.47	1.09
ST100-30	68.0	–	4.0	6.8	0.76	2.91
75:25-0	67.7	33.4	1.6 1.9 1.4	6.4	0.091	10.5
75:25-30	69.5	33.4	2.1 2.6 2.2	6.4	0.053	10.0
50:50-30	49.7	33.0	1.5 1.8 1.5	7.1	0.060	22.0
25:75-30	49.8	33.1	1.6 1.5 1.8	7.1	0.11	32.7
BG100-30	–	33.3	1.8 1.6 1.8	–	0.083	100
		Average:		6.8 ± 0.5	0.08 ± 0.03	

\*S-SC: slow-spectral component; F-SC: fast-spectral component.

strating that this molecular order is robust. The disappearance of the peak at  $2\theta = 11.3$  upon addition of glycerol may indicate that the glycerol may facilitates a polymorphic transition or that the formed crystallites are very small. Similar diffractions in cellulose nanocrystals have cross-sectional dimensions of a few nanometers, which make their diffraction patterns sensitive to size and orientation (Newman et al., 2013). The glycerol might help a normal orientation of the film profile, reducing the signal from the 110-crystal plane family.

The diffraction data collected for all the films prove that the melting allows a complete transformation of the ST. In fact, after the casting, the A-type crystalline polymorphs typical for the native ST part was absent and only B-type and Vh-type polymorphs were detected. As the ST content raised, we found a gradual increase of the peaks associated with the ST crystal morphology (Fig. 2). This increase indicates that the ST and the BG appeared as discrete phases in the films and did not interact.

The chemical heterogeneity and dynamics in the films can be detected in highly hydrated environments by EPR. Electron para-

magnetic resonance is widely used to study polymeric materials in terms of morphology, heterogeneity, structural transformations, chain dynamics (Bender & Berliner, 2004; Kruczala, Varghese, Bokria, & Schlick, 2003; Kruczala, Wasim, & Schlick, 2005; Schlick & Jeschke, 2012). EPR detects paramagnetic centers and the stability of these in the solids is an advantage for the analysis. Analysis of polymeric materials usually requires use of external spin probes (Kruczala et al., 2003; Kruczala et al., 2005; Kruczala & Szajdzińska-Piętek, 2015). In our previous work, copper was used as a spin probe to identify heterogeneity in ST granules as an effect of ST phosphate esters (Blennow et al., 2006). The EPR spectrum of the nitroxyl radicals in TEMPO comprises three lines due to the hyperfine interaction of unpaired electron spin with the nuclear spin of  $^{14}\text{N}$

(I=1) (Valić, Andreis & Klepac, 2011). These interactions are affected by the chemical environment. Hence, EPR using TEMPO as external spin probe allows to monitor the chain dynamics in the polysaccharide with different chemical structures, in this specific case at different ST to BG ratios.

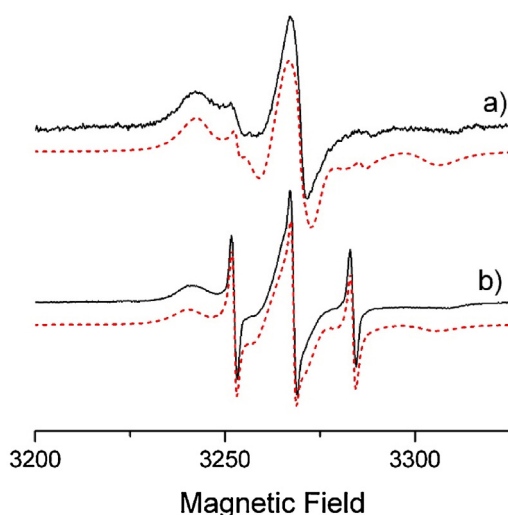


**Fig. 3.** EPR spectra of the spin probe in casted prototypes: A) ST100-0. B) 75:25-0. Black line- experimental spectra, red dotted line-simulated spectra. (For interpretation of the references to colour in this figure legend, the reader is referred to the web version of this article.)

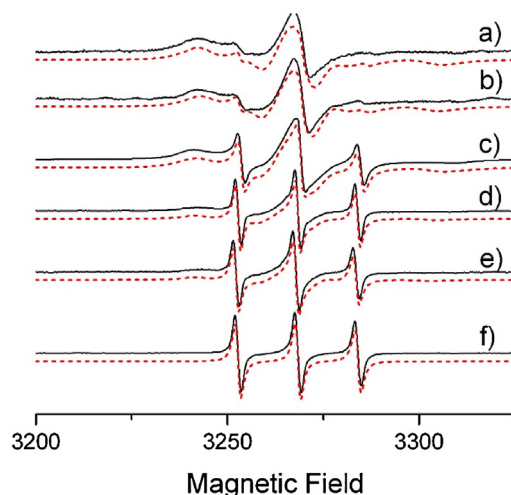


**Fig. 4.** EPR spectra of the spin probe in films: a) ST100-0. b) ST100-30. c) 75:25-30. d) 50:50-30. e) 25:75-30. f) BG100-30. Black line: experimental spectra, red dotted line: simulated spectra. (For interpretation of the references to colour in this figure legend, the reader is referred to the web version of this article.)

The spectrum for pure ST film comprised only one component characterized by extreme separation (ES) of 65.5 G (Table 1). This rotation is related to a spin probe in the restrained phase i.e. rigid amorphous phase, possibly related to the semi-crystalline nature of the films (Kruczala et al., 2003). When the amount of BG increased in the blends, the dynamically fast (F) component emerged. If the spin probe is located both in flexible and rigid phases, fast and slow motional components can be observed in the composite EPR spectrum (Fig. 3B). EPR spectra from all ST:BG samples were found to be a superposition of two main components, due to a slow (S-SC) and a fast-spectral component (F-SC) (Fig. 4). By increasing the BG content in the ST films, the intensity of F-SC component increased. The 100% BG had only F-SC (Fig. 4). All the EPR spectra were simulated using Easy Spin software with  $A_{1\text{so}} = 16.15 \pm 0.25$  G and  $g_{1\text{so}} = 2.0056 \pm 0.0002$  and rotational correlation times ( $\tau_c$ ) given in Table 1. The minor variation of  $A_{1\text{so}}$  and  $g_{1\text{so}}$  suggests that both environments (responsible for S-SC and F-SC) exhibited similar polarity. The calculated rotational correlation times for the probe located in pure ST ( $\tau_c = 6.8 \pm 0.5$  ns) did not change in presence of BG, suggesting

that two separate phases are formed. Also  $\tau_c$  for F-SC for pure BG and mixed ST:BG was very similar ( $\tau_c = 0.08 \pm 0.03$  ns) supporting our hypothesis. The result suggests that ST and BG do form significant entanglement. The films of pure ST with and without glycerol showed a small sharp tree line ERP signal. However, the correlation time for the first was 5–7 time higher than for BG samples indicating the presence of a small amount (1–2%) of mobile, amorphous phase in pure ST.

This behavior indicates that BG and ST formed separate phases in which the BG phase is more mobile and more amorphous. This additive effect was confirmed by the WAXS data shown above.

Likewise, the slow component, attributed mostly to semi-crystalline ST regions, was also confirmed by specific reflexions in the WAXS spectra. The addition of glycerol showed a decreased amount of S-SC, which further supports the formation of a looser structure in the glycerol plasticized films. Increasing the glycerol concentration from 23% to 30% did not show any different EPR signal suggesting that the effects of glycerol at the concentrations used were saturating. This effect may be related to the formation of larger mobile volumes generating looser structures.

### 3.3. Mechanical properties

The casted films were evaluated by tensile tests to characterize their deformation behavior. The results obtained for stress at break, strain at break and Young's modulus were compared as functions of glycerol and BG (Fig. 5). The effect of glycerol was evident at all the ST:BG ratios and for all the mechanical parameters tested (Fig. 5). The strain at break ( $\epsilon_r$ ) increased with increased glycerol content (Fig. 5C). The comparison between the ST100 films with both 23% and 30% glycerol did not show major differences. However, for the samples with increasing amount of BG the strain at break increased significantly. The films without glycerol showed a maximum elongation that was not correlated to the ST:BG ratio. Increased amount of BG resulted in higher cohesiveness and stiffness of the films. This effect, as confirmed by the Young's moduli (Fig. 5B), documented the high stiffness of the samples with BG in the formulation. In all cases, the glycerol decreased the stiffness of the films.

The stress at break (Fig. 5A) of the films without glycerol showed similar results for ST100-0 and BG100-0. Partial substitution of ST with BG imparted an increased resistance to the applied force. This was evident in the increased stress at break for the films with high BG content (Fig. 5A). The addition of 23% or 30% glycerol plasticizer to the pure ST film decreased the stress at break 5-fold. Similar decreases were found for the ratios ST:BG-Gly, 50:50-30, 25:75-30 and BG100-30 with 30% glycerol, with the exception of the ratio 75:25-30 (2-fold decrease, Fig. 5A). All blends and the pure BG films with 23% glycerol showed in average a 2-fold decrease in stress at break as compared to the films without plasticizer. This result demonstrated that the robustness of the film can be optimized using low amounts of BG. The comparison between the stress/strain values for the ST100 and the 75:25 films with and without glycerol (Fig. 5D) showed that the BG in a ST-based film improved the mechanical properties, increasing resistance and elasticity. Glycerol considerably influenced the crystalline and mechanical properties of the films. The stress at break and Young's modulus decreased with increasing amount of glycerol included in the films, having a minimum for the films at ST:BG ratio of 50:50. This result is probably correlated with the plasticizing action of the glycerol. The plasticizer can create void volumes inside the matrix structure causing a decrease in stiffness and strength of the films. This effect was correlated with increasing amount of glycerol (Fig. 5A,B). The addition of glycerol also profoundly influenced the elongation of the films increasing with increasing amount of glycerol. This effect is also correlated with increased BG content. Interestingly, the effect of BG on the elongation was detected only

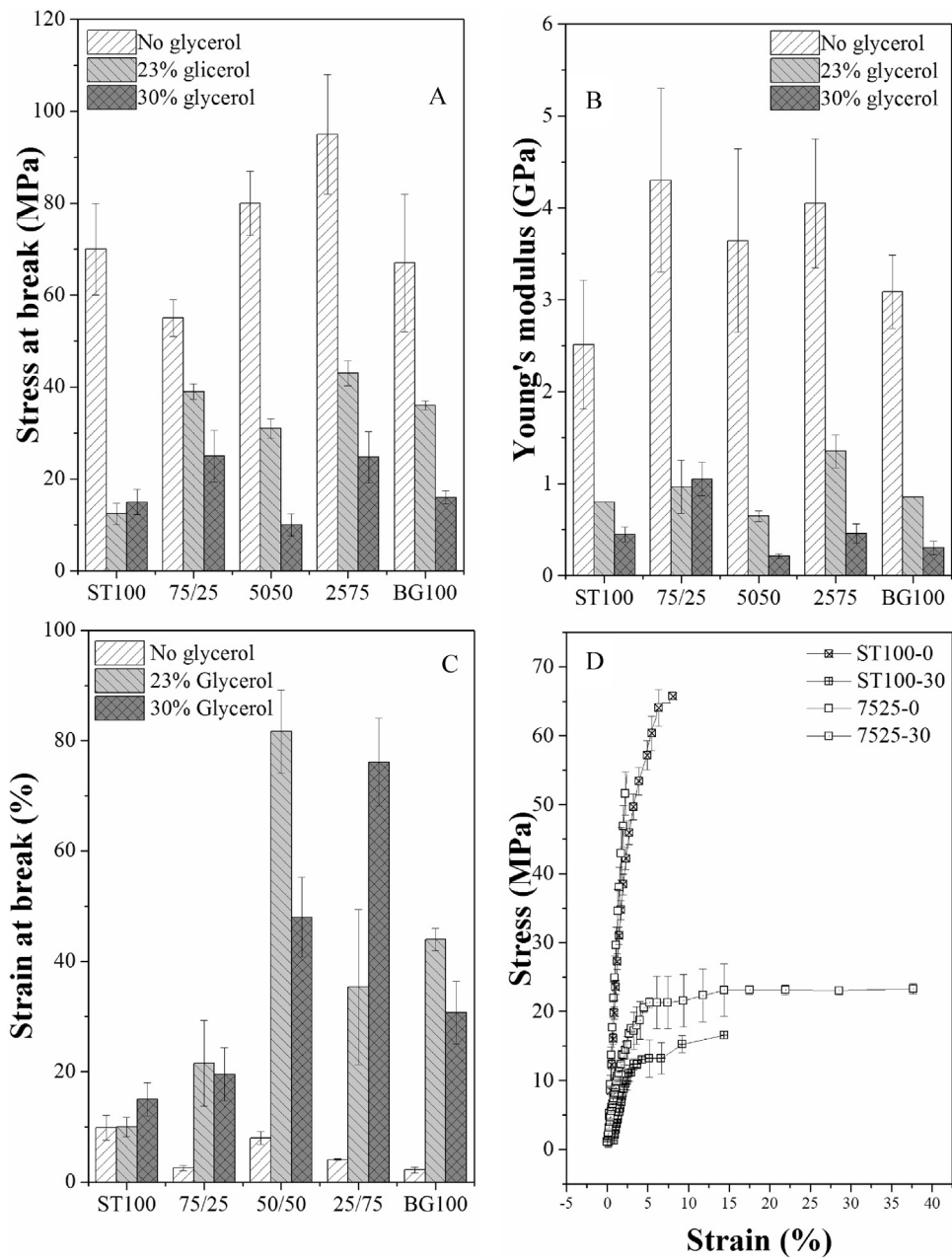


**Fig. 5.** Mechanical properties of ST:BG-gly films as a function of glycerol and BG content. A) Overlay of stress at break (%). B) Overlay of Young's modulus (MPa). C) Overlay of strain at break for all prototype. D) Stress and strain curves of selected prototypes.

with the addition of glycerol. This data suggested a higher affinity of this plasticizer to BG. However, the relationships were complex and the 50:50 ratios had a maximum elongation at 23% glycerol while the 25:75 ratios had a maximum elongation at 30% glycerol.

#### 3.4. Effects of temperature and humidity on dynamic visco-elasticity

The casted films were analyzed for their visco-elastic properties using a dynamic mechanical analyzer (DMA). Storage ( $E'$ ) and loss moduli ( $E''$ ) were measured using the tension mode and by applying gradients of both temperature and RH. The temperature gradient mode permitted the estimation of the glass transition temperature by comparing the derivative of the storage modulus and the  $\tan \delta$  peak. As expected from its plasticizing effect, all films, except for the pure BG films, showed lower glass transition temperature ( $T_g$ )

with increasing glycerol content. The pure BG films had a lower glass transition temperature than pure ST. However, these films did not show any sensitivity to the glycerol in decreasing the  $T_g$  (Table 2). Furthermore, the presence of BG did not have any effect on the  $T_g$  of the composite films. Increased glycerol content caused an increasing in the hygroscopicity of the films. Furthermore, the water had a concerted effect with the plasticizer in decreasing the glass transition. The comparison between 23% and 30% did not show any significant effect.

The storage modulus  $E'$  measured at 20 °C for different RH conditioning for all ST:BG compositions demonstrates that the RH leads to decreased  $E'$ , which indicates a water plasticizing effect of both ST and BG (Fig. 6). In correspondence to a 70–80% humidity a faster decrease of  $E'$  was detected. This corresponded to the glass transition effect, at ambient temperature. As compared to the fairly large variation within each sample, the modulus did not vary much in

**Table 2**

Glass transition ( $T_g$ ) temperatures of composites and pure polysaccharide films. (\*) single measurements.

	Tg 0% glycerol	Water content (%)	Tg 23% glycerol	Water content (%)	Tg 30% glycerol	Water content (%)
ST100	90 ± 6	10	80*	23	69*	23
BG100	65 ± 1	13	65 ± 2	20	65*	25
75:25	100 ± 3	10	70 ± 5	20	70 ± 8	20
50:50	90*	10	68*	22	64*	20
25:75	107*	10	71*	23	75 ± 3	23

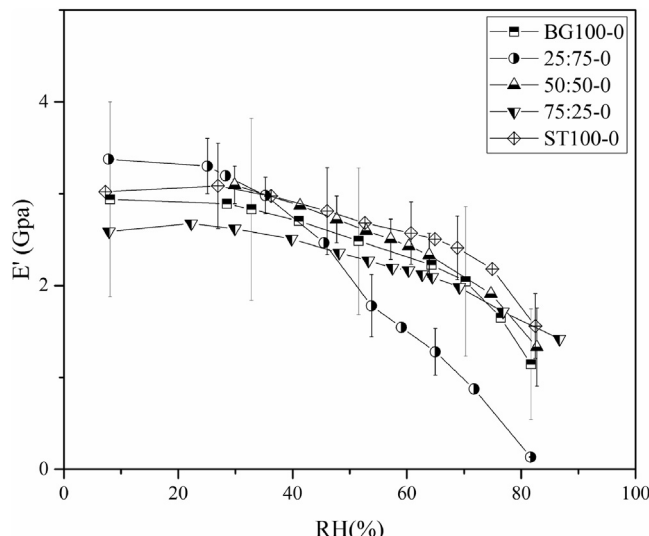


**Fig. 6.** Storage modulus as a function of a RH demonstrating that the composites storage modulus ( $E'$ ) were not influenced by the BG content.

function of the film composition. Generally, the  $E'$  was 2.5–3.5 GPa at low RH, and slightly lower, 1–2 GPa, at high RH. These values are in the same order as the  $E'$  measured at high deformation level. This trend was similar for all compositions excepted for sample 25:75 for which modulus surprisingly decreased more rapidly than others at 30% RH and higher.

### 3.5. Gas permeability

Water vapor,  $\text{CO}_2$  and  $\text{O}_2$  permeability measurements were carried out on casted films. Films casted using only starch in absence of glycerol were too brittle and fragile to be tested. However, films with glycerol were more flexible and had interesting properties, especially in terms of water vapor permeability. For films with 23% glycerol, the permeability to water vapor decreased with reducing of the starch content. The pure starch films showed a permeability of  $0.35 \text{ cm}^3 \text{ mm}/\text{m}^2 24 \text{ h kPa}$ . The films with ratios ST:BG-Gly of 50:50-23, 25:75-23 and BG100-23 showed permeability of 0.1, 0.1 and  $0.05 \text{ cm}^3 \text{ mm}/\text{m}^2 24 \text{ h kPa}$ , respectively. The 8-fold lower permeability for pure BG, as compared to pure ST films, demonstrated an important role of BG in reducing the water vapor permeability. The values for the 30% glycerol films were in the range of

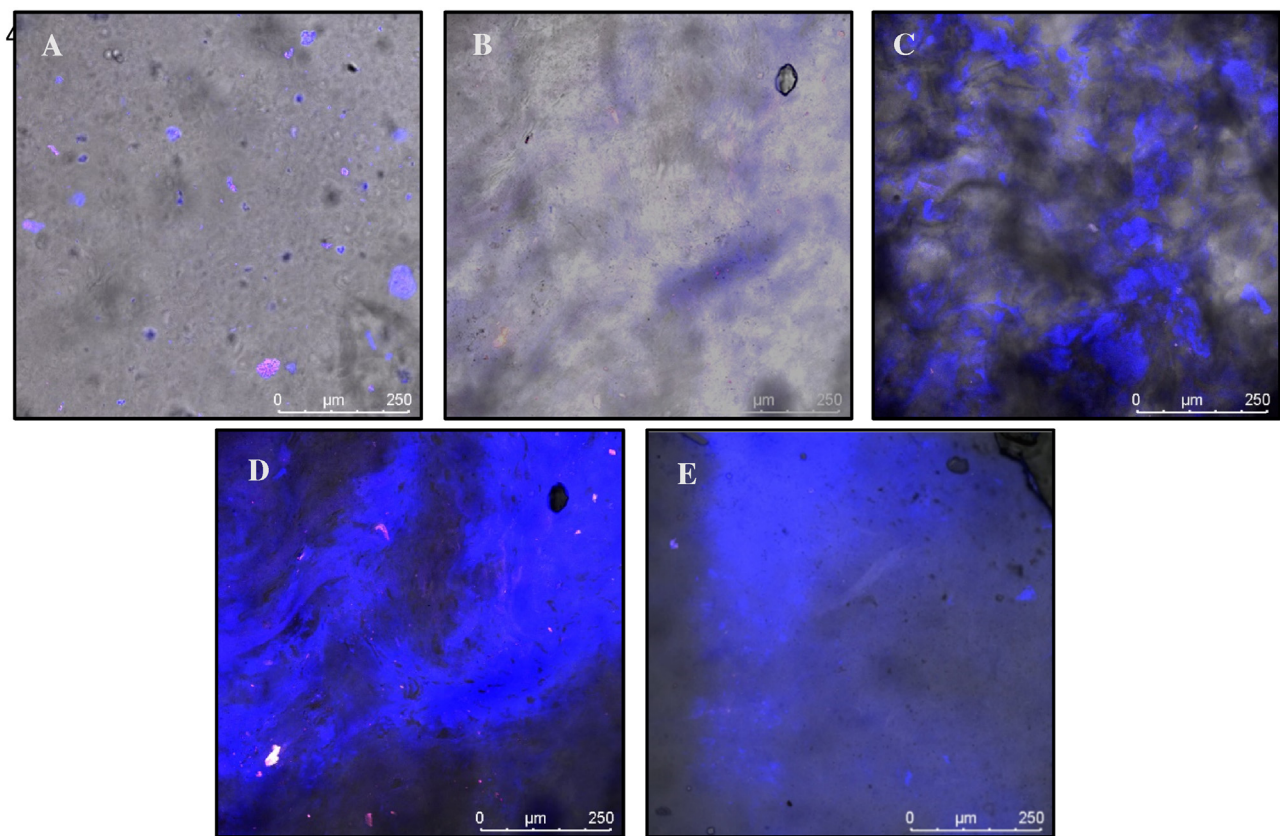


**Fig. 7.** Analysis of the films dyed with calcofluor demonstrating ST:BG-Gly phase partitioning. BG: blue fluorescence, ST: bright field gray/dark. Fluorescent spots in A are contaminating cell wall fragments in the ST. A) ST100-0. B) 75:25-0. C) 50:50-0. D) 25:75-0. E) BG100-0. (For interpretation of the references to colour in this figure legend, the reader is referred to the web version of this article.)

0.1 cm<sup>3</sup> mm/m<sup>2</sup> 24 h kPa regardless of the concentrations of BG utilized. The CO<sub>2</sub> and O<sub>2</sub> permeability did not show any significant difference with BG content (CO<sub>2</sub>: ~0.3 cm<sup>3</sup> mm/m<sup>2</sup> 24 h kPa O<sub>2</sub>: ~5 cm<sup>3</sup> mm/m<sup>2</sup> 24 h kPa).

### 3.6. Surface and internal analyses of the film analyzed by confocal microscopy

The inner structure of the composite prototypes, as analyzed by confocal laser scanning microscopy (CLSM), showed a complex texture for all the specimens. The films stained simultaneously with calcofluor and iodide solutions revealed a ST:BG phase partitioning for composite films (Fig. 7B–D; Supplementary Fig. S1). This result confirmed both the crystallography data, demonstrating separate and additive effects on the crystallinity of the films, and the EPR data, suggesting the presence of regions with separated molecular mobility characteristics. The BG100 film showed a homogeneous surface as validated by bright field microscopy (Supplementary Fig. S1). However, the ST100 film showed a relatively smooth surface but spotted calcofluor fluorescence (Fig. 7A; Supplementary Fig. S1), as indicated by the presence of trace residual maize cell wall fragments. Generally, we expect that minor impurities including lipids, protein and cell wall fragments can possibly and disturb the matrix decreasing permeability to water and gasses and also affect the Young's modulus, e.g. slightly decrease the stiffness of pure starch films.

## 4. Conclusions

Thermoplastic composites fabricated by blending maize ST and oat BG were tested as models for all-natural and edible bio-plastics. The raw starch, but not BG, showed typical melting transition as determined by DSC. ST had an A-type crystalline polymorph while BG contained cellulose-type crystallites. Casted films showed additive ST:BG crystalline structures. BG decreased the crystallinity of the composite films. Glycerol specifically reduced a very broad reflection at approx. 2θ = 11°. EPR spectra revealed the presence of well separated fast and slow molecular mobility components, specific for BG and ST, respectively. Most importantly, the composite films had improved mechanical performances, characterized by increased stress at break and Young's moduli, as compared to the pure ST films. Important relationships were revealed between WAXS, EPR and mechanical data. Notably, the decrease in the starch-related A-type polymorphs by addition of BG as showed by WAXS correlated to molecularly more open structures as suggested by EPR. These data corroborate with the increased elasticity at high BG contents even if this effect was mainly detected in the presence of glycerol. However, the Tg did not decrease significantly and E' measured at variable RH did not change. BG increased the barrier properties to water vapor of films. The data support the development of ST:BG blend composites as a possible all-natural and edible alternative to synthetic polymer blends.

## Acknowledgements

We would like to thank Marianne Lund Jensen for technical help. We would also like to thank the Center for Advanced Bioimaging, Faculty of Science, the University of Copenhagen for use of their microscopy facilities. This work was funded by The Danish Council for Independent Research Technology and Production Sciences and Carlsberg Foundation.

## Appendix A. Supplementary data

Supplementary data associated with this article can be found, in the online version, at <http://dx.doi.org/10.1016/j.carbpol.2017.05.043>.

## References

- ASTM. (2010). *Standard test method for oxygen gas transmission rate through plastic film and sheeting using a coulometric sensor*. pp. D3985. ASTM.
- ASTM. (2011). *Standard test method for water vapor transmission rate through plastic film and sheeting using a modulated infrared sensor*. pp. F1249. ASTM.
- Bender, C. J., & Berliner, L. J. (Eds.). (2004). *Biological magnetic resonance* (Vol. 21). New York, NY: Kluwer Academic/Plenum Publishing Corporation.
- Bastioli, C., Bellotti, V., Del Giudice, L., & Grilli, G. (1993). Mater-bi: Properties and biodegradability. *Journal of Polymers and the Environment*, 1, 181–191.
- Blennow, A., Houborg, K., Andersson, R., Bidzinska, E., Dyrek, K., & Łabanowska, M. (2006). Phosphate positioning and availability in the starch granule matrix as studied by EP. *Biomacromolecules*, 7, 965–974.
- Blennow, A., Jensen, S. L., Shaik, S. S., Skryhan, K., Carciofi, M., Holm, P. B., et al. (2013). Future cereal starch bioengineering: cereal ancestors encounter gene technology and designer enzymes. *Cereal Chemistry Journal*, 90(4), 274–287.
- Burton, A. R., & Fincher, B. G. (2012). Current challenges in cell wall biology in the cereals and grasses. *Frontiers in Plant Science*, 3, 1–6.
- Follain, N., Joly, C., Dole, P., & Blizard, C. (2005). Mechanical properties of starch-based materials. I. Short review and complementary experimental analysis. *Journal of Applied Polymer Science*, 97, 1783–1794.
- Garcia, V., Colonna, P., Lourdin, D., Buleon, A., Bizot, H., & Ollivon, M. (1996). Thermal transitions of cassava starch at intermediate water contents. *Journal of Thermal Analysis*, 47(5), 1213–1228.
- Gemen, R., de Vries, J. F., & Slavin, J. L. (2011). Relationship between molecular structure of cereal dietary fiber and health effects: focus on glucose/insulin response and gut health. *Nutrition Reviews*, 69(1), 22–33.
- Giosafatto, C. V. L., Di Pierro, P., Gunning, P., Mackie, A., Porta, R., & Mariniello, L. (2014). Characterization of Citrus pectin edible films containing transglutaminase-modified phaseolin. *Carbohydrate Polymers*, 106, 200–208.
- C. V. L. Giosafatto, P. Di Pierro, P. Gunning, A. Mackie, R. Porta, L. Mariniello. (2014) Trehalose-containing hydrocolloid edible films prepared in the presence of transglutaminase. *Biopolymers* 101, 931–937.
- Hebelstrup, K. H., Sagnelli, D., & Blennow, A. (2015). The future of starch bioengineering: GM microorganisms or GM plants? *Frontiers in Plant Science*, Hindleah, A. M. (1980). X-ray characterization of viscose rayon and the significance of crystallinity on tensile properties. *Textile Research Journal*, 50(10), 581–589.
- Jantanasakulwong, K., Leksawasdi, N., Seesuriyachan, P., Wongsuriyasak, S., Techapun, C., & Ougizawa, T. (2016). Reactive blending of thermoplastic starch, epoxidized natural rubber and chitosan. *European Polymer Journal*, 84, 292–299.
- Kruczala, K., & Szajdzińska-Pietek, E. (2015). Electron paramagnetic resonance spectroscopy and forward recoil spectrometry chapter in characterization of polymer blends. In S. Thomas, Y. Grohens, & P. Jyotishkumar (Eds.), *Miscibility, morphology and interfaces*. Wiley-VCH.
- Kruczala, K., Varghese, B., Bokria, J. G., & Schlick, S. (2003). Thermal aging of heterophasic propylene-ethylene copolymers: morphological aspects based on ESR, ESR imaging and FTIR. *Macromolecules*, 36(6), 1899–1908.
- Kruczala, K., Wasim, A., & Schlick, S. (2005). Stabilization and early degradation of UV-irradiated heterophasic propylene-ethylene copolymers based on ESR ESR imaging, UV-vis, and DSC: Effect of ethylene content and UV wavelength. *Macromolecules*, 38(16), 6979–6987.
- Lazaridou, A., & Biliaderis, C. G. (2007). Molecular aspects of cereal β-glucan functionality: Physical properties, technological applications and physiological effects. *Journal of Cereal Science*, 46(2), 101–118.
- Lazaridou, A., Biliaderis, C. G., Micha-Screttas, M., & Steele, B. R. (2004). A comparative study on structure-function relations of mixed-linkage (1-3), (1-4) linear β-D-glucans. *Food Hydrocolloids*, 18(5), 837–855.
- Lourdin, D., Della Valle, G., & Colonna, P. (1995). Influence of amylose content on starch films and foams. *Carbohydrate Polymers*, 27, 261–270.
- Lourdin, D., Bizot, H., & Colonna, P. (1997). 'Antiplasticization' in starch-glycerol films? *Journal of Applied Polymer Science*, 63, 1047–1053.
- Mariniello, L., Giosafatto, C. V. L., Di Pierro, P., Sorrentino, A., & Porta, R. (2010). Swelling, mechanical and barrier properties of albedo-based films prepared in the presence of phaseolin crosslinked or not by transglutaminase. *Biopolymers*, 11, 2394–2398.
- Myllarinen, P., Partanena, R., Seppala, J., & Forssell, P. (2002). Effect of glycerol on behaviour of amylose and amylopectin <sup>1</sup>H NMR. *Carbohydrate Polymers*, 50, 355–361.
- Mikkelsen, M. S., Jespersen, B. S., Larsen, F. H., Blennow, A., & Engelsen, S. B. (2013). Molecular structure of large-scale extracted β-glucan from barley and oat: Identification of a significantly changed block structure in a high β-glucan barley mutant. *Food Chemistry*, 136, 130–138.
- Montero, B., Rico, M., Rodríguez-Llamazares, S., Barral, L., & Bouza, R. (2016). Effect of nanocellulose as a filler on biodegradable thermoplastic starch films from tuber, cereal and legume. *Carbohydrate Polymers*, 157, 1094–1104.
- Newman, R. H., Hill, J. S., & Harris, P. J. (2013). Wide-angle X-ray scattering and solid-state nuclear magnetic resonance data combined to test models for cellulose microfibrils in mung bean cell walls. *Plant Physiology*, 163, 1515–1558.

- Ovecka, M., Bahaji, A., Muñoz, F. J., Almagro, G., Ezquer, I., Baroja-Fernández, E., et al. (2012). A sensitive method for confocal fluorescence microscopic visualization of starch granules in iodine stained samples. *Plant Signaling & Behavior*, 7(9), 1146–1150.
- Pérez, S., Baldwin, P. M., & Gallant, D. J. (2009). *Structural features of starch granules I. Starch* (3rd ed.). Elsevier.
- Sagnelli, D., Hebelstrup, K. H., Leroy, E., Rolland-Sabaté, A., Guillois, S., Kirkensgaard, J. J. K., et al. (2016). Plant-crafted starches for bioplastics production. *Carbohydrate Polymers*, 152, 398–408. <http://dx.doi.org/10.1016/j.carbpol.2016.07.039>
- Schlick, S., & Jeschke, G. (2012). *Polymer science: A comprehensive reference*. pp. 221. Elsevier.
- Valič, S., Andreis, M., & Klepac, D. (2011). ESR spectroscopy of multiphase polymer systems. In A. Boudenne, L. Ibos, Y. Candau, & S. Thomas (Eds.), *Handbook of multiphase polymer systems*. 2011: John Wiley & Sons Ltd.
- Zuluaga Gallego, R., Putaux, J.-L., Castro Herazo, C., Vélez, J. M., Mondragon, I., Miner, A. R., et al. (2014). *Cellulose microfibrils isolated from musaceae fibrous residues cellulose based composites*. pp. 43–61. Wiley-VCH Verlag GmbH & Co. KGaA.